J Appl Electrochem (2009) 39:477–483
DOI 10.1007/s10800-008-9668-2

ORIGINAL PAPER

Comparison of the electrochemical properties of intermediate temperature solid oxide fuel cells based on protonic and anionic electrolytes

Daniela La Rosa · Massimiliano Lo Faro · Giuseppe Monforte · Vincenzo Antonucci · Antonino Salvatore Aricò

Revised: 18 September 2008 / Accepted: 18 September 2008 / Published online: 26 September 2008

Abstract The physico-chemical properties of two protonic electrolytes $BaCe_{0.8}Y_{0.2}O_{3-\delta}$ and $BaCe_{0.9}Y_{0.1}O_{3-\delta}$ were investigated. The $BaCe_{0.8}Y_{0.2}O_{3-\delta}$ electrolyte showed better crystallographic purity and lower amount of carbonate phase on the surface. A comparison between the $BaCe_{0.8}Y_{0.2}O_{3-\delta}$ protonic electrolyte supported cell and an anionic ($Ce_{0.8}Gd_{0.2}O_{1.95}$) one was made. The maximum power densities (IR-free) of 183 mW cm^{-2} and 400 mW cm^{-2} were obtained in H_2 (R.H. 3%) at 700 °C, for the protonic and anionic electrolyte based cells, respectively.

Keywords AC-Impedance · $BaCe_{0.8}Y_{0.2}O_{3-\delta}$ · $Ce_{0.8}Gd_{0.2}O_{1.95}$ · Protonic conductors · Solid oxide fuel cells

1 Introduction

Solid oxide fuel cells (SOFCs) convert chemical energy into electrical energy with high efficiency and low pollutant emission levels [1, 2]. As opposed to low temperature fuel cells these high temperature fuel cell systems can directly use hydrocarbons as fuels besides hydrogen and they are CO tolerant [3–10]. CO is usually one of the contaminants of hydrogen produced from fossil fuels. However, significantly higher temperatures (~800–1000 °C) are necessary for the electrolytes to be sufficiently conductive to sustain fuel cell operation at reasonable power levels. Thus, these systems suffer from materials related problems. In this regard, in order to overcome the associated drawbacks of the SOFC systems, a new series of proton-conducting ceramic materials based on the perovskite structure has been developed [11–16].

In recent years, protonic conductors have been widely studied due to their suitable protonic conductivity at intermediate temperatures. These oxides can work in the temperature range 400–750 °C and they represent a possible alternative to the classical SOFC electrolytes based on yttria stabilized zirconia which operates only at higher temperatures. Ceramic proton conductors have a larger ionic transport number than ceria doped gadolinia and better chemical compatibility with conventional SOFC materials than lanthanum strontium gallates (LSGM). Both CGO and LSGM are promising candidates as anionic electrolytes for intermediate temperature operation. Ceramic proton conducting electrolytes thus compete with anionic CGO and LSGM for application in intermediate temperature solid oxide fuel cells. The possibility to operate at lower temperatures presents several advantages such as easier cell construction, the use of cheaper hardware materials and the reduction of thermal stress.

In this work, two formulations of barium cerate-based protonic electrolytes have been studied ($BaCe_{0.8}Y_{0.2}O_{3-\delta}$ and $BaCe_{0.9}Y_{0.1}O_{3-\delta}$). The drawbacks related to the use of these materials have been discussed. In addition, a comparison between two cells with the same electrode configuration but equipped with different electrolytes, one protonic (BCYO) and the other anionic (CGO), is presented.

D. La Rosa (✉) · M. Lo Faro · G. Monforte · V. Antonucci · A. S. Aricò
CNR-ITAE Institute, Via Salita S. Lucia Sopra Contesse 5, 98126 Messina, Italy
e-mail: larosa@itae.cnr.it

2 Experimental

2.1 Preparation of substrates

Dense $BaCe_{0.8}Y_{0.2}O_{3-\delta}$ and $BaCe_{0.9}Y_{0.1}O_{3-\delta}$ substrates were prepared from their ceramic powders (Praxair). Each powder was ball-milled for 14 h, and then uniaxially pressed into pellets in a die under a pressure of 400 MPa. The thickness of the pellet was controlled at 300 μm by using an appropriate amount of BCYO powder. The green pellets were sintered at 1450 °C for 6 h to obtain dense substrates. The density was larger than 95% of theoretical value. After the thermal treatment a color change was observed. In fact, the samples turned from white to black. The same phenomenon is reported in the literature [17, 18] for anionic electrolytes based on lanthanum gallate with a perovskite structure. However, from a careful analysis of their diffraction patterns this does not seem to be related to the presence of secondary phases. A slight formation of Ce^{3+} ions is not excluded [19]. Yet, this does not appear to affect the open circuit voltage of the SOFC cells equipped with these protonic electrolytes.

The thermal treatment was carried out in N_2 atmosphere in order to reduce the formation of carbonates. In fact, the high basicity of these oxides is advantageous for the formation of protonic charge carriers but, on the other hand, basic oxides are expected to react easily with acidic or even amphoteric gases like SO_3, CO_2, H_2O to form the respectively sulfates, carbonates and hydroxides [20]. CGO electrolytes were prepared as reported elsewhere [21].

2.2 Physico-chemical characterization of the films

X-ray diffraction (XRD) analyses were carried out on the precursor powders as well as the thick substrates (300 μm) after the thermal treatment. A X'PERT Philips diffractometer equipped with a copper target (Cu Kα radiation source) was used.

X-ray photoelectron spectroscopy (XPS) analyses were carried out on the surface of the pellets after the thermal treatment. A Physical Electronics GmbH-System ESCA 5800 spectrometer equipped with monocromatic Al Kα X-ray electron source and flood-gun neutralizer was used.

2.3 Electrical characterization

The protonic materials were electrically characterized in conductivity cells fed with wet air (Relative Humidity (R.H.) 3%). Silver electrodes were deposited by painting on the two sides of the electrolyte pellet and then thermally heated in order to solder the contacts. Gold wires were used as current collectors.

The protonic conductivity is commonly determined by impedance spectroscopy which allows the bulk resistance to be determined from the complex impedance plot (high frequency intercept on the Nyquist plot).

In this study, ac-impedance measurements were performed in the temperature range 150–800 °C using an AUTOLAB PGSTAT 30. Impedance spectra were obtained in the frequency range 10 mHz to 1 MHz with applied ac-voltage amplitude of 10 mV rms. The resistance values obtained from the impedance spectra were used to calculate the conductivities of barium cerate-based electrolytes. The same approach was used for CGO electrolytes.

Moreover, in order to estimate the ionic transport number the protonic electrolytes properties were investigated at both 600 °C and 800 °C in a SOFC device fed with a mixture of $Ar–H_2$ at the anode and static air at the cathode. The open circuit voltage values were measured at different H_2 concentrations in the range 0–100% after appropriate conditioning and compared to those obtained with CGO electrolytes in the presence of silver electrodes at the same temperature.

In order to evaluate the performance of a cell based on a protonic electrolyte a SOFC device fed with hydrogen was tested at different temperatures. The protonic cell used in this study had the following architecture:

Anode: Cermet of a Ni on LSFCO catalyst (70 wt.%) and $BaCe_{0.8}Y_{0.2}O_{3-\delta}$ (30 wt.%) (thickness: 15 μm)

Electrolyte membrane: $BaCe_{0.8}Y_{0.2}O_{3-\delta}$ (thickness: 300 μm)

Cathode: LSFCO ($La_{0.6}Sr_{0.4}Fe_{0.8}Co_{0.2}O_3$) (thickness: 15 μm)

The anionic cell used in this study had the same architecture and anode and cathode materials but $BaCe_{0.8}Y_{0.2}O_{3-\delta}$ was replaced by CGO. It was preferred to use a Ni-doped perovskite at the anode to favour the compatibility with the perovskite structure of the electrolyte. The stabilization of LSFCO under mild reducing conditions at the anode has been discussed in literature [7].

The procedure for the preparation of the electrolyte pellets has been described above.

The LSFCO cathode was deposited by spraying with isopropanol. The deposit was fired at 1100 °C for 2 h. The anode containing a mixture of calcined Ni/LSFCO catalyst (70%wt.) and 30% (wt.) of electrolyte was also deposited by spraying using the same organic vehicle as for the cathode and thermally treated at 1100 °C for 2 h in air. Finally, the SOFC cell was mounted on an alumina tube, sealed with ceramic adhesive (AREMCO 516) and heated to 800 °C in air. A gold paste (Hereaus) and gold wires were used to form both anode and cathode current collectors.

The anode was fed with humidified H_2 (R.H. 3%). The cathode was exposed to stationary air. The electrochemical analysis was performed with a Metrohm Autolab 30

apparatus equipped with a FRA (frequency response analyzer) and 20 Ampere booster.

3 Results and discussion

3.1 XRD and XPS analyses of the samples

Figure 1a shows a comparison between the X-ray diffractograms of the $BaCe_{0.8}Y_{0.2}O_{3-\delta}$ powder and the pellet after the thermal treatment at 1450 °C. In Fig. 1b the same comparison is shown for the $BaCe_{0.9}Y_{0.1}O_{3-\delta}$ electrolyte. XRD spectra related to the two formulations in the as received powders showed a small presence of $BaCO_3$ carbonate phase in the bulk as revealed from a peak at about 24° 2θ. A good crystallographic and compositional purity, especially in the pellets was observed. The crystallographic peaks associated with carbonates disappeared after the high temperature treatment. In the pellet with the highest amount of Y (20%Y) a shift of the diffraction peaks towards higher Bragg angles was observed; this indicates a lattice contraction.

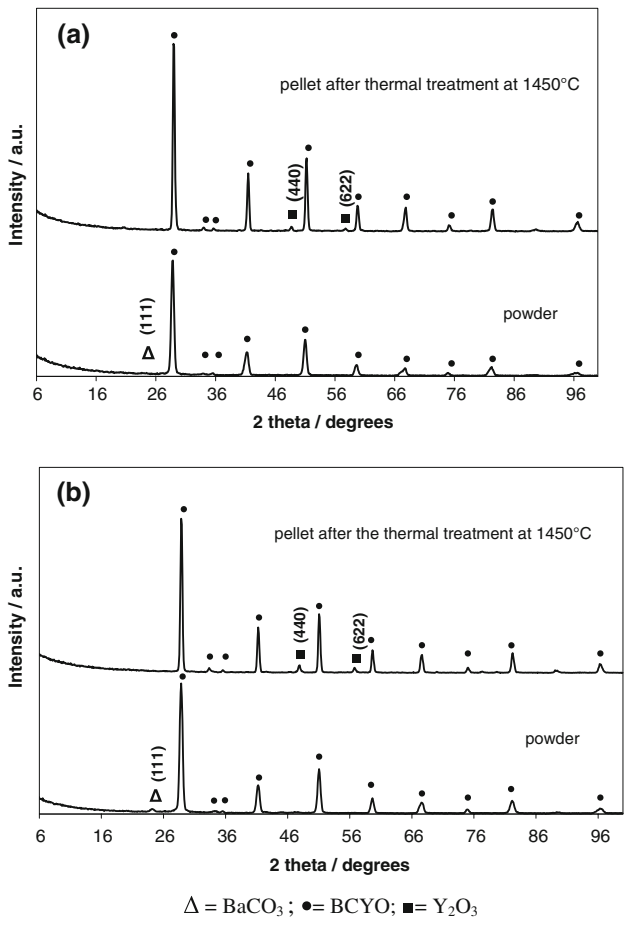

Fig. 1 X-ray diffraction patterns of: **a** $BaCe_{0.8}Y_{0.2}O_3$ before and after the thermal treatment; **b** $BaCe_{0.9}Y_{0.1}O_3$ before and after the thermal treatment

In order to investigate whether contamination by carbonate was still present after the high temperature treatment in inert atmosphere, the sample was subject to XPS analysis.

Figures 2 and 3 show the XPS spectra of the $BaCe_{0.8}Y_{0.2}O_{3-\delta}$ and $BaCe_{0.9}Y_{0.1}O_{3-\delta}$ pellets. The peak at 289 eV in the C 1s spectra suggests the presence of a small amount of carbonate on the surface. This signal is significantly smaller in the $BaCe_{0.8}Y_{0.2}O_{3-\delta}$ vs. $BaCe_{0.9}Y_{0.1}O_{3-\delta}$ sample. Due to the better crystallographic purity the $BaCe_{0.8}Y_{0.2}O_{3-\delta}$ sample was selected for further analyses.

3.2 Conductivity measurements

The conductivity of the protonic conductor with increasing temperature was recorded at 100 °C intervals (except for the first point obtained at 150 °C) in a wet hydrogen (R.H. 3%) atmosphere. The bulk conductivity values for the $BaCe_{0.8}Y_{0.2}O_{3-\delta}$ electrolyte are reported in an Arrhenius plot (Fig. 4) in order to also determine the activation energy for proton conduction. The conductivity values of CGO electrolytes used in the present work were previously determined [22]. For comparison they are reported in the plot of Fig. 4. The $BaCe_{0.8}Y_{0.2}O_{3-\delta}$ electrolyte has a conductivity of 3.2×10^{-3} S cm^{-1} at 700 °C. This value is lower than the corresponding one obtained for an anionic electrolyte such as $Ce_{0.8}Gd_{0.2}O_{1.95}$ [23–26]. The conductivity of the protonic electrolyte is smaller than that reported in the literature [27]. This may be in part related to the different R.H. values adopted for the measurements.

Possibly, the conductivities of the barium cerate-based materials could be further increased by complete elimination of the small traces of the insulating $BaCeO_3$ phase.

The activation energy for $BaCe_{0.8}Y_{0.2}O_{3-\delta}$ obtained from the slope of the Arrhenius plot is 0.4 eV; this agrees with the literature [28]. Moreover, this value is considerably lower than those observed for the anionic electrolytes (0.8 eV) [29]; this indicates a lower activation with temperature and, consequently, the possibility to operate at low temperatures.

In order to estimate the ionic transport number properties of the protonic electrolytes, these were also characterized in a SOFC device fed with a mixture of Ar/H_2 (3% H_2O) at the anode and static air at the cathode. Silver electrodes at both faces of the pellet were used in these experiments. The open circuit potential values obtained at different H_2 concentrations and at a temperature of 600 °C are plotted in Fig. 5. As shown in Fig. 5, upon increasing the H_2 concentration, the OCV increases from a value of about 50 mV to a value of 1.14 V. This latter is comparable to the thermodynamic value for 100%

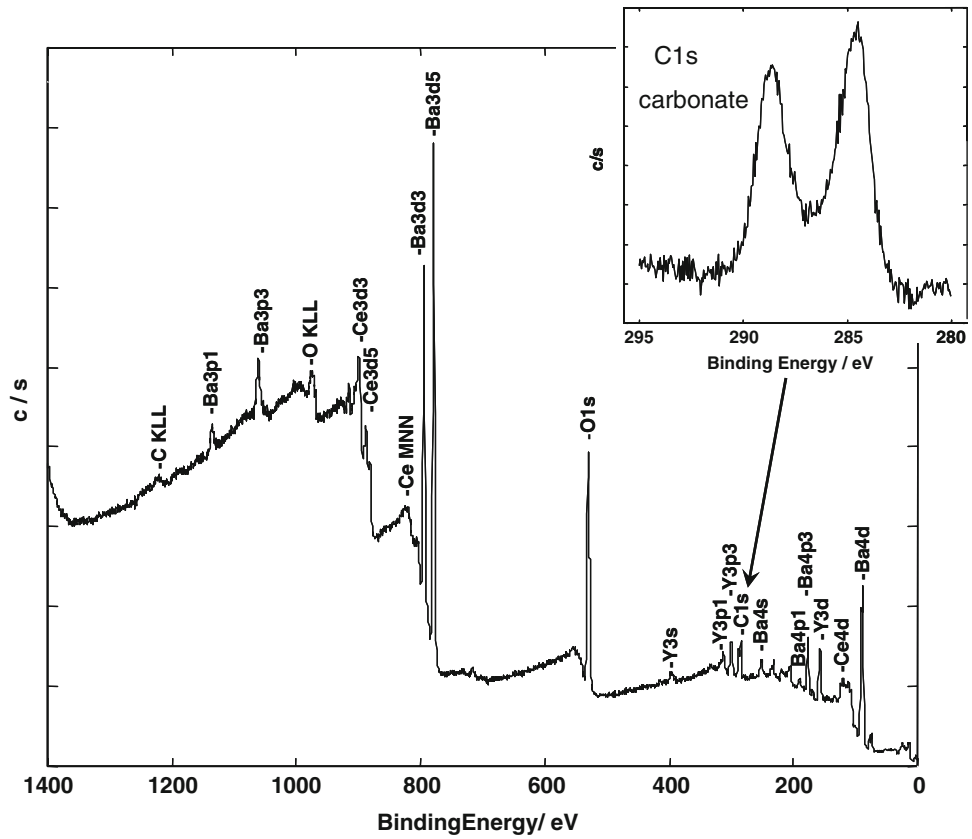

Fig. 2 XPS spectrum of $BaCe_{0.8}Y_{0.2}O_3$ after the thermal treatment

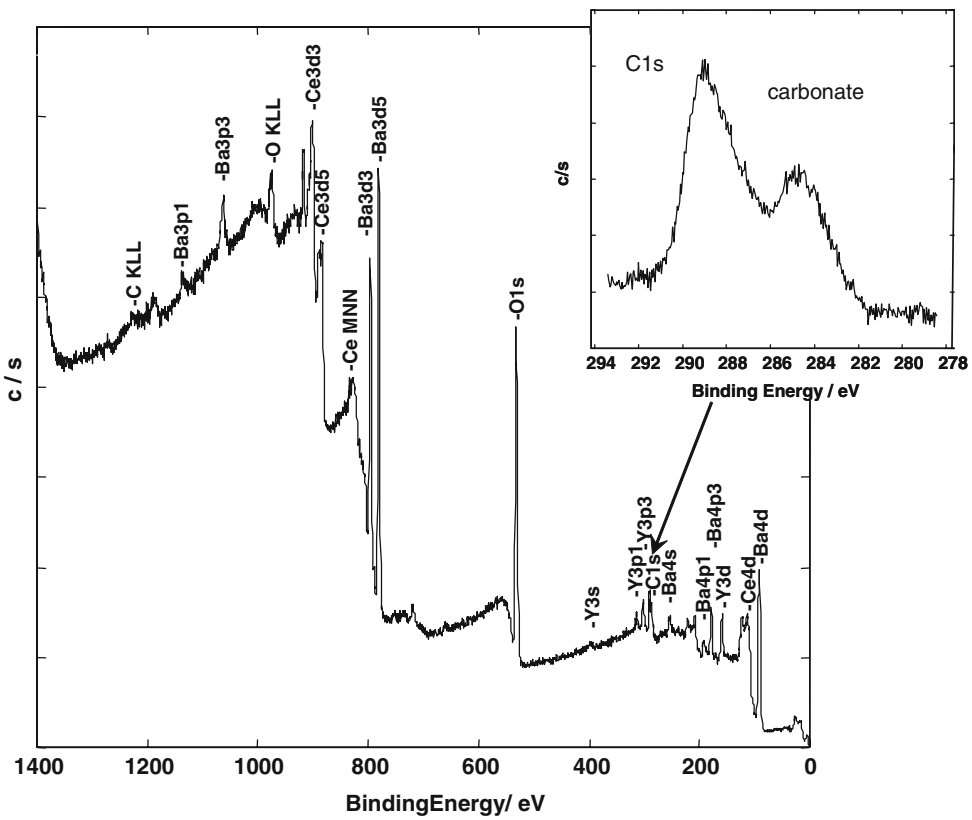

Fig. 3 XPS spectrum of $BaCe_{0.9}Y_{0.1}O_3$ after the thermal treatment

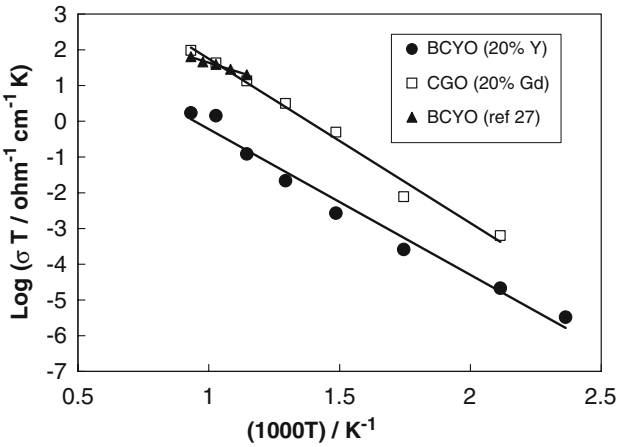

Fig. 4 Arrhenius plot of BCYO (20% Y), BCYO (ref. [27]) and CGO (20% Gd) bulk conductivities

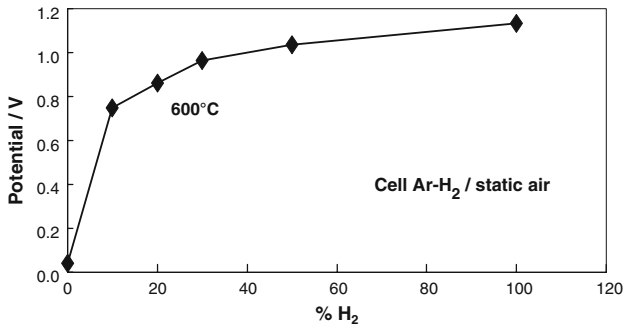

Fig. 5 Open circuit potential measurements obtained for $BaCe_{0.8}Y_{0.2}O_3$ samples

H_2/air. Thus, it seems that the ionic transport number is roughly unity. This is not the case for CGO where, under the same conditions, an OCV value of 0.85 V was achieved [30], which would correspond to an ionic transport number of about 0.8. Thus, a significant fraction of energy is lost at low current densities owing to a parasitic electron transport through the electrolyte ($Ce^{4+} \leftrightarrow Ce^{3+}$ process). As envisaged by Steele [19], this effect for CGO is less significant at high currents due to the presence of weaker reducing conditions.

Finally, two cells with the same electrodes but with a different electrolyte were electrochemically characterized. The thickness of the electrolyte was 300 μm in both cases. The results were compared in order to evaluate the differences in performance between a protonic electrolyte based-cell and an anionic cell with same electrodes and architecture.

Ac impedance spectra of the BCYO ($BaCe_{0.8}Y_{0.2}O_{3-\delta}$) supported cell operating in the presence of H_2 in the range 700–800 °C are shown in Fig. 6. The series resistance (Rs) derived from the high frequency intercept on the real axis

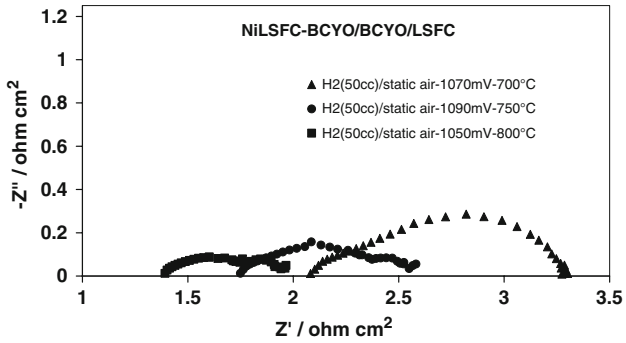

Fig. 6 Comparison between the impedance spectra obtained in the range 700–800 °C for the BCYO supported cell

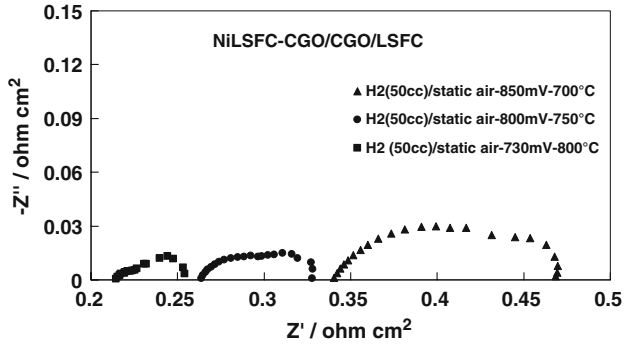

Fig. 7 Comparison between the impedance spectra obtained in the range 700–800 °C for the CGO supported cell

of the Nyquist plot decreases from 2.1 Ω cm^2 at 700 °C to 1.38 Ω cm^2 at 800 °C.

Ac impedance spectra of the CGO supported cell are shown in Fig. 7. The series resistance decreases from 0.34 Ω cm^2 at 700 °C to 0.21 Ω cm^2 at 800 °C. It appears that the series resistance of the cell based on the CGO electrolyte is significantly smaller than that of the cell equipped with the protonic electrolyte at all temperatures. This effect is mainly due to the better ionic conductivity of CGO compared to BCYO.

The charge transfer resistance (RCT) was obtained by the difference between the low and high frequency intercept on the Nyquist plot. RCT is often associated with activation polarization for low overpotential. The RCT is quite similar for CGO and BCYO electrolyte based cells at 700 °C, but is significantly smaller (one half) for the CGO cell at 800 °C. The ac-impedance profiles consist of two main semicircles for both systems but, the profiles are quite different for the two cells at 700 °C. In the BCYO cell, the semicircle at low frequency, mainly related to the cathode contribution, shows large impedance values, whereas, in the CGO based cell the semicircle at high frequency that is related to the anode prevails in terms of impedance. In this latter system the reduction of Ce^{4+} to Ce^{3+} plays a significant role, causing a parasitic current

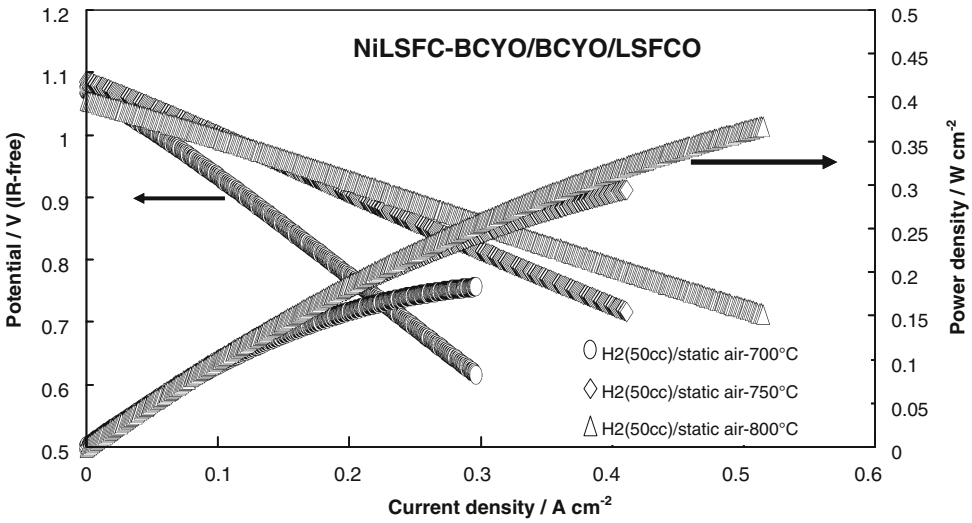

Fig. 8 Comparison between the IR-free polarization curves obtained in the range 700–800 °C for the BCYO supported cell

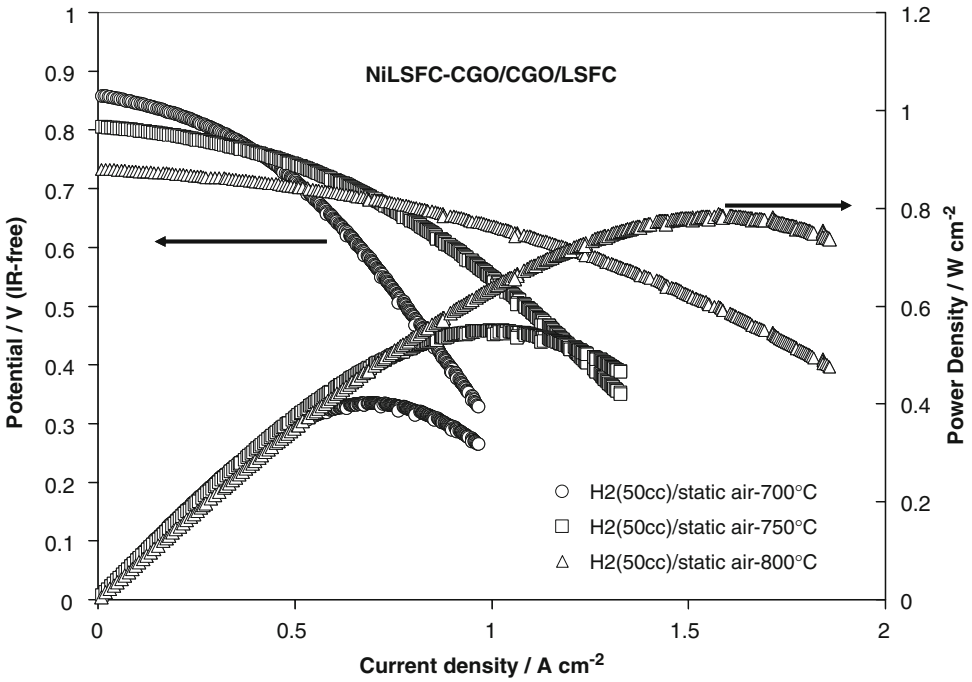

Fig. 9 Comparison between the IR-free polarization curves obtained in the range 700–800 °C for the CGO supported cell

through the electrolyte. The different ac-impedance profiles indicate a significant role of the electrode-electrolyte interface. As the performance of the BCYO cell is strongly affected by the ohmic resistance of the electrolyte, in order to obtain a reliable comparison between the two cells in terms of interface characteristics, the IR-free polarization curves were calculated from raw polarization data. In Figs. 8 and 9 the IR-free polarization curves related to the BCYO and CGO cells are shown. The maximum power densities obtained at 700 °C were 183 mW cm^{-2} for the BCYO based-cell and 400 mW cm^{-2} for the CGO cell. Table 1 summarizes IR-free power density data obtained at different temperatures for the two cells. The performances obtained for the anionic electrolyte supported cell are about twice higher than the protonic one. As stated by Steele [19] the effect of parasitic electron drag is significant for CGO electrolytes at conditions close to the OCV. At low current densities the BCYO cell performs better than the CGO cell due to the higher ionic transport number. However, the low current density zone is not of practical interest. At reasonable current densities and cell voltages e.g. 0.7 V the CGO cell performs better than the BCYO cell even at 700 °C. Due to its lower activation energy, it is likely that, at temperatures below 700 °C e.g. in the range 400°–600 °C, the protonic may outperform the anionic electrolyte cell. However, at present, the performance recorded at such low temperatures does not appear to be of practical interest.

Table 1 Comparison between the power densities obtained at different temperatures for the BCYO and CGO based cells

T (°C)	Power density (mW cm^{-2})	Power density (mW cm^{-2})
700	183	400
750	294	546
800	367	784

4 Conclusions

The physico-chemical properties of two protonic electrolytes $BaCe_{0.8}Y_{0.2}O_{3-\delta}$ and $BaCe_{0.9}Y_{0.1}O_{3-\delta}$ have been investigated. The $BaCe_{0.8}Y_{0.2}O_{3-\delta}$ electrolyte showed better crystallographic purity and a lower amount of carbonate phase on the surface.

Comparison between the $BaCe_{0.8}Y_{0.2}O_{3-\delta}$ protonic electrolyte supported cell and an anionic (CGO) one was made. The maximum power densities (IR-free) of 183 mW cm^{-2} and 400 mW cm^{-2} were obtained in H_2 (R.H. 3%) at 700 °C, for the protonic and anionic electrolyte based cells, respectively.

The performance of the CGO cell, after ohmic drop correction, is about twice that of the proton conductor based cell in the temperature range 700–800 °C. It appears from ac-impedance that this difference in behaviour is associated with superior cathode/electrolyte interface for the CGO cell.

From a practical point of view the anionic electrolytes present advantages with respect to the protonic ones in the range of temperature higher than 700 °C both in terms of anionic conductivity and electrode/electrolyte interface. On the other hand, the CGO cell likely suffers from parasitic electron drag at low current densities due to the low ionic transport number.

The performance of a protonic electrolyte solid oxide fuel cell may be improved by using a thin film electrolyte and appropriate cathode material optimized for operation with a proton conducting electrolyte. The results obtained with optimized protonic electrolyte SOFC cells at low temperatures highlight the possibility of developing an intermediate temperature fuel cell capable of closing the gap between PEM and classical SOFC/MCFC systems. However, there obviously exists a need for continued improvement in material conductivity and rigorous testing of these materials, especially those with higher chemical stability.

Acknowledgment The authors are grateful to the Italian Ministry of Education and Research (MIUR) for financial support through the FISR project.

References

1. Singhal SC (2000) Solid State Ionics 135:305
2. Yamamoto O (2000) Electrochim Acta 45:2423
3. Lu C, Worrell WL, Wang C, Park S, Kim H, Vohs JM, Gorte RJ (2002) Solid State Ionics 152–153:393
4. Lu C, An S, Worrell WL, Vohs JM, Gorte RJ (2004) Solid State Ionics 175:47
5. Zhu W, Xia C, Fan J, Peng R, Meng G (2006) J Power Sources 160:897
6. An S, Lu C, Worrell WL, Gorte RJ, Vohs JM (2004) Solid State Ionics 175:135
7. Sin A, Kopnin E, Doubitsky Y, Zaopo A, Aricò AS, Gullo LR, La Rosa D, Antonucci V (2005) J Power Sources 145:68
8. Sin A, Kopnin E, Doubitsky Y, Zaopo A, Aricò AS, Gullo LR, La Rosa D, Antonucci V (2006) Fuel Cells 6:137
9. Lo Faro M, La Rosa D, Monforte G, Antonucci V, Aricò AS, Antonucci P (2007) J Appl Electrochem 37:203
10. Sin A, Kopnin E, Doubitsky Y, Zaopo A, Aricò AS, Gullo LR, La Rosa D, Antonucci V (2007) J Power Sources 164:300
11. Yajima T, Iwahara H, Uchida H (1991) Solid State Ionics 47:117
12. Iwahara H, Uccida H, Ono K, Ogaki KJ (1988) J Electrochem Soc 135:529
13. Slade RCT, Singh N (1991) Solid State Ionics 46:111
14. Stevenson DA, Jiang N, Buchanan RM, Henn FEG (1993) Solid State Ionics 62:279
15. Bonanos N (2001) Solid State Ionics 145:265
16. Suksamai W, Metcalfe IS (2007) Solid State Ionics 178:627
17. Rambabu B, Ghosh S, Zhao W, Jena H (2006) J Power Sources 159:21
18. Djurado E, Labeau M (1998) J Eur Ceram Soc 18:1397
19. Steele BCH (2000) Solid State Ionics 129:95
20. Kreuer KD (1997) Solid State Ionics 97:1
21. Herle JV, Horita T, Kawada T, Sakai N, Yokokawa H, Dokiya M (1998) Ceram Int 24:229
22. Sin A, Kopnin E, Doubitsky Y, Zaopo A, Aricò AS, Gullo LR, La Rosa D, Antonucci V, Oliva C, Ballabio O (2004) Solid State Ionics 175:361
23. Tianshu Z, Hing P, Huang H, Kilner J (2002) Solid State Ionics 148:567
24. Christie GM, Van Berkel FPF (1996) Solid State Ionics 83:17
25. Torrens RS, Sammes NM (1998) Solid State Ionics 111:9
26. Doshi R, Carter JD (1999) J Electrochem Soc 146:1273
27. Iwahara H (1996) Solid State Ionics 86–88:9
28. Ma G, Shimura T, Iwahara H (1998) Solid State Ionics 110:103
29. Inaba H, Tagawa H (1996) Solid State Ionics 83:1
30. Pérez-Coll D, Marrero-López D, Ruiz-Morales JC, Núñez P, Abrantes JCC, Frade JR (2007) J Power Sources 173:291